Applied Nanoscience (2020) 10:1331–1343
https://doi.org/10.1007/s13204-019-01235-7

ORIGINAL ARTICLE

Fabricating carbon nanofibers from a lignin/r-PET blend: the synergy of mass ratio with the average fiber diameter

Efstratios Svinterikos[1] · Ioannis Zuburtikudis[2] · Mohamed Al-Marzouqi[1]

Received: 27 September 2019 / Accepted: 6 December 2019 / Published online: 17 December 2019

Abstract

For the first time, we map the conditions that lead to the successful preparation of carbon nanofibers from a blend of lignin and recycled poly(ethylene terephthalate) (r-PET). Particularly, we describe how their morphology depends on the synergy between the lignin/r-PET mass ratio and the average fiber diameter of the precursor fibers. Electrospun mats consisting of different lignin/r-PET mass ratios (from 50/50 to 90/10) and different average fiber diameters (from 80 to 400 nm) were prepared. After carbonizing them to 600 °C, it was repeatedly observed that the samples having a relatively high mass ratio of r-PET (> 33 wt%) and low average fiber diameters (~ 100 nm) exhibit extensive melting and the fibrous structure collapses. In contrast, samples of the same high mass ratio of r-PET but large average fiber diameters (> 300–400 nm) yield infusible filamentous carbon structures. This nano-dimension phenomenon declines when the r-PET content is low enough (~ 10 wt%). In this case, the nanofibers are practically infusible and carbon nanofibers with average diameters close to 100 nm and a well-formed filamentous structure are produced. Such thin lignin-based carbon nanofibers have scarcely been reported. The reasons leading to the melting of the nanofibrous mats which consist of certain mass ratios and average fiber diameters are related to variations in the decomposition rates of the two precursor polymers and also to differences in their crystallization. These phenomena are explained based on experimental results from thermogravimetry, X-ray diffraction and differential scanning calorimetry. Moreover, BET surface area measurements indicate that the melting of nanofibrous mats compromises the porosity of the activated carbon nanofibers produced from them, while the presence of r-PET has a positive impact on the development of porosity.

Keywords Lignin · Recycled PET · Electrospinning · Carbon nanofibers

Introduction

The utilization of biorenewable and waste materials for the manufacture of high added-value products has emerged as an issue of increased importance in the era of escalating environmental concerns, which drive the need for the development of the circular economy.

Lignin is the second most abundant natural polymer on Earth behind cellulose (Ruiz-Rosas et al. 2010; Frank et al. 2014). It is a major natural source of aromatic compounds and it represents around 25–30% of the total non-fossil organic molecules on our planet (Thakur et al. 2014; Alekhina et al. 2015). Industrially, lignin is derived as a by-product of the paper industry, although only a minor amount of its total annual production is used for the manufacture of commercial products (Ruiz-Rosas et al. 2010; Frank et al. 2014). It is a biodegradable, natural feedstock, compatible with a variety of chemicals. However, its heterogeneous structure, which depends on the plant source and the method of extraction, limits its more extensive use. Lignin is commonly classified as a low-cost material, especially when it is used as a carbon fiber precursor, as it is compared with the more costly polyacrylonitrile (Baker and Rials 2013; Frank et al. 2014). However, the price of lignin increases if it is treated further, e.g. when it is purified or fractionated,

Electronic supplementary material The online version of this article (https://doi.org/10.1007/s13204-019-01235-7) contains supplementary material, which is available to authorized users.

✉ Ioannis Zuburtikudis
ioannis.zuburtikudis@adu.ac.ae

[1] Department of Chemical and Petroleum Engineering, United Arab Emirates University (U.A.E.U.), Al Ain, UAE

[2] Department of Chemical Engineering, Abu Dhabi University, Abu Dhabi, UAE

depending on the desired application. In this research, lignin was used as it was received from the supplier without any further treatment.

Poly(ethylene terephthalate) (PET) is one of the most common commodity plastics and one of the most widely recycled plastic in the USA in terms of weight (NAPCOR 2018). As the global consumption of plastics rises annually by 5–6% (Wang et al. 2015), the development of alternative uses for the plastic waste, and especially for recycled PET, will be instrumental in upgrading the municipal waste management.

Due to its relatively high carbon content and its large availability, lignin has been proposed as a biorenewable feedstock for the manufacture of carbon fibers and nanofibers (Frank et al. 2014). Carbon fibers are a filamentous form of carbon, widely employed for the manufacture of composites for the automotive industry (Frank et al. 2014; Peng et al. 2016; Zhang et al. 2016). When their diameter is reduced in the nano-scale, they are termed as carbon nanofibers (CNFs). The minimization of the fiber diameter maximizes their surface area, a property which makes a difference in applications such as adsorption, catalysis and energy storage. The most common procedure for the manufacture of CNFs from polymeric precursors is based on the spinning of the precursors into nanofibers, followed by their thermal treatment at temperatures higher than 600 °C under inert atmosphere (carbonization) (Inagaki et al. 2012). One of the most well-established techniques for the spinning of polymeric precursors into nanofibers is electrospinning. Using this technique, the polymer (or a mixture of polymers) is initially dissolved in a suitable solvent and then the polymer solution flows at a controlled rate through a syringe under the influence of an electrostatic field. The electrostatic force stretches and elongates the jet and as the solvent evaporates, nanofibers are formed (Ko and Wan 2014a).

In a previous article of our team, we have described the feasibility of carbon nanofiber fabrication from a blend of lignin with recycled PET (r-PET) (Svinterikos and Zuburtikudis 2016). First, these two polymers are dissolved in the same solvent (trifluoroacetic acid) at certain mass ratios and solution concentrations. Then they are spun into nanofibers using the electrospinning technique and, finally, they are carbonized for their transformation into CNFs.

Lignin is a highly branched polymer which is built by the polymerization of three phenylpropane units (guaiacyl, syringyl and p-hydroxyphenyl; G, S and H unit respectively) (Fig. 1a, b). (Wool and Sun 2005; Duval and Lawoko 2014). The configuration of the lignin structure and the relative quantity of each of its three building monomers vary among plant species (Zhang et al. 2012; Frank et al. 2014). Lignin derived from hardwoods mainly consists of S and G units, while lignin originating from softwoods primarily consists of G and small amounts of H units (Zhang et al. 2012; Frank et al. 2014). For the same lignin that we have used in our research (kraft lignin with low sulfonate content purchased from Sigma-Aldrich, product number #471003), Zhang et al. have estimated that the relative proportion of the three monomers constituting the lignin structure is $H_{10.3}G_{35.8}S$ (Zhang et al. 2012). Thus, G constitutes around 78% of its building monomers and the amount of S is negligible. Other studies using the same lignin that we have used here suggest

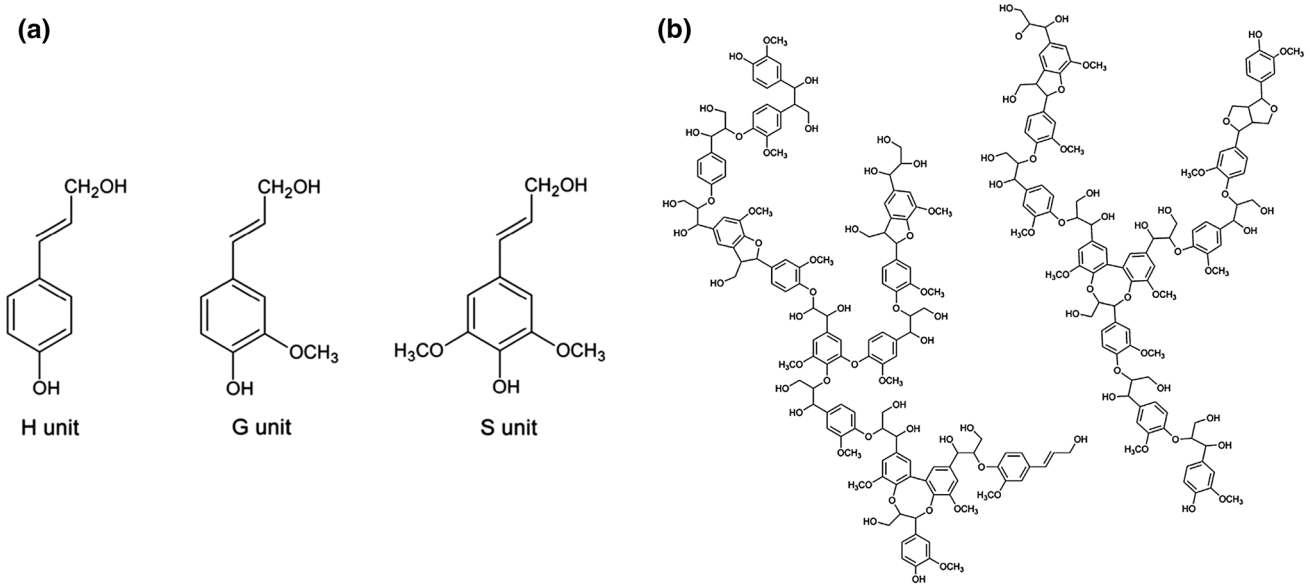

Fig. 1 **a** The three lignin monomer units; **b** representative structure of softwood lignin (Duval and Lawoko 2014)

a similar relative ratio between C, O and H in its structure (Jönsson et al. 2018; Mohabeer et al. 2019).

The branched configuration makes lignin amorphous (Svinterikos and Zuburtikudis 2016). Therefore, it doesn't melt during heating under inert atmosphere, but it slowly decomposes at a multi-stage process (Rodríguez Correa et al. 2017). In contrast, PET consists of linear chains, which built a semicrystalline structure. Upon heating, PET melts at around 240–250 °C, and decomposes at a single stage near 400–410 °C (Svinterikos et al. 2019). Due to similarities in their monomer units, when these two polymers are blended their chains interact through weak van der Waals forces and they are miscible at a dimensional scale between 5 and 15 nm (Kadla and Kubo 2004).

Attempting to produce CNFs from lignin with r-PET, we have observed that the production of CNFs with a well-formed filamentous structure is only possible under certain conditions regarding the mass ratio between lignin and r-PET and the average diameter of the precursor electrospun nanofibers. In this article, we describe the conditions leading to the successful fabrication of CNFs, while we illuminate the reasons leading to the collapse of the fibrous structure when these conditions are not met. The average fiber diameters (close to 100 nm) reported here, are among the lowest that have been reported for lignin-based CNFs.

Experimental part

The lignin feedstock that was used in this research is kraft lignin purchased from Sigma-Aldrich (#471003, Mw ~ 10,000 g/mol, low sulfonate content), and it was used as received. The source of recycled PET (r-PET) was waste water bottles, which came from the same bottling company in the UAE. The Melt Flow Index (MFI) of the recycled PET was measured to be 72 g/10 min at 260 °C with 2.16 kg load (measurement with a Chengde Jingmi (XRL-400) plastometer according to ASTM D1238). The water bottles were left to dry and then they were cut into small pieces, in order to be dissolved in trifluoroacetic acid for the electrospinning solutions. The electrospinning solvent (trifluoroacetic acid, 99%) was purchased from Merck. Both polymers were dissolved together under certain mass ratios and at certain concentrations (see below) for producing electrospun mats with desirable average fiber diameters. The lignin/r-PET solutions were left under magnetic stirring at room temperature for at least 12 h, until they were homogeneously dissolved. Electrospinning was performed using a FUENCE E-sprayer (ES-2000S) apparatus in which the setup has vertical orientation.

Our purpose was to investigate the impact of two parameters on the carbonization of the electrospun nanofibrous mats; the lignin/r-PET mass ratio and the average fiber diameter of each electrospun mat. The range of lignin/r-PET mass ratios investigated here was between 50/50 and 90/10. Successful attempts to electrospin lignin alone have been previously reported, when Alcell lignin in ethanol is used (Lallave et al. 2007; García-Mateos et al. 2017). However, our attempts to fabricate electrospun fibers of lignin alone here were unsuccessful; instead only spray was formed. This has been previously reported for kraft lignin in several occasions, and it has been explained on the basis of its relatively low Mw and the lack of chain entanglements which would otherwise raise the solution viscosity to the point of balancing the stretching force of the electrostatic field (Choi et al. 2013; Jin et al. 2014). Therefore, increasing the lignin/r-PET mass ratio to more than 90/10 induced spinnability problems here. Moreover, at mass ratios lower than 50/50 the carbonization yield becomes rather low and also the fibers melt due to the presence of the semicrystalline r-PET. So, we kept the mass ratio between 50/50 and 90/10.

Electrospun mats of different average fiber diameter (D) in the range 80–400 nm were produced by varying the solution concentration (the concentration of both polymers into the solution) in the range of 9–25% w/v. It was not feasible to prepare bead-free fibrous mats with D lower than 80 nm. The conditions leading to the preparation of the desired electrospun mats have been previously published by our team (Svinterikos and Zuburtikudis 2017; Svinterikos et al. 2019).

In total, 12 electrospun samples were prepared for the investigation of the melting behavior; 4 samples consisting of 50/50 lignin/r-PET mass ratio with D of 80 nm, of 245 nm, of 308 nm and of 387 nm respectively; 3 samples consisting of 67/33 lignin/r-PET mass ratio with D of 97 nm, of 176 nm and of 320 nm; 3 samples consisting of 80/20 lignin/r-PET mass ratio with D of 97 nm, of 136 nm and of 279 nm; finally, 2 samples consisting of 90/10 lignin/r-PET mass ratio with D of 95 nm and of 152 nm. For all the electrospun samples the voltage was kept at 30 kV, the spinning distance at 7.7 cm and the flow rate at 0.1 μL/min. The choice of these values was based on our previous studies (Svinterikos and Zuburtikudis 2017; Svinterikos et al. 2019).

Each electrospun sample was carbonized in a temperature-programmed tubular furnace (Tube Furnace GSL-1500X-50, MTI) under inert atmosphere (N_2) at a heating rate of 5 °C/min until it reached 600 °C, where it was held for 1 h.

The morphology of each electrospun mat and of each carbonized mat was examined using Scanning Electron Microscopy (SEM) (JEOL Neoscope JCM-5000) after coating them with gold. The average fiber diameter of each sample was measured using an image analyzer (ImageJ, National Institute of Health, USA).

The thermogravimetric analysis (TGA) of the samples was carried out using a TA Q500 instrument at inert atmosphere (N_2). The heating rate was 7 °C/min and the

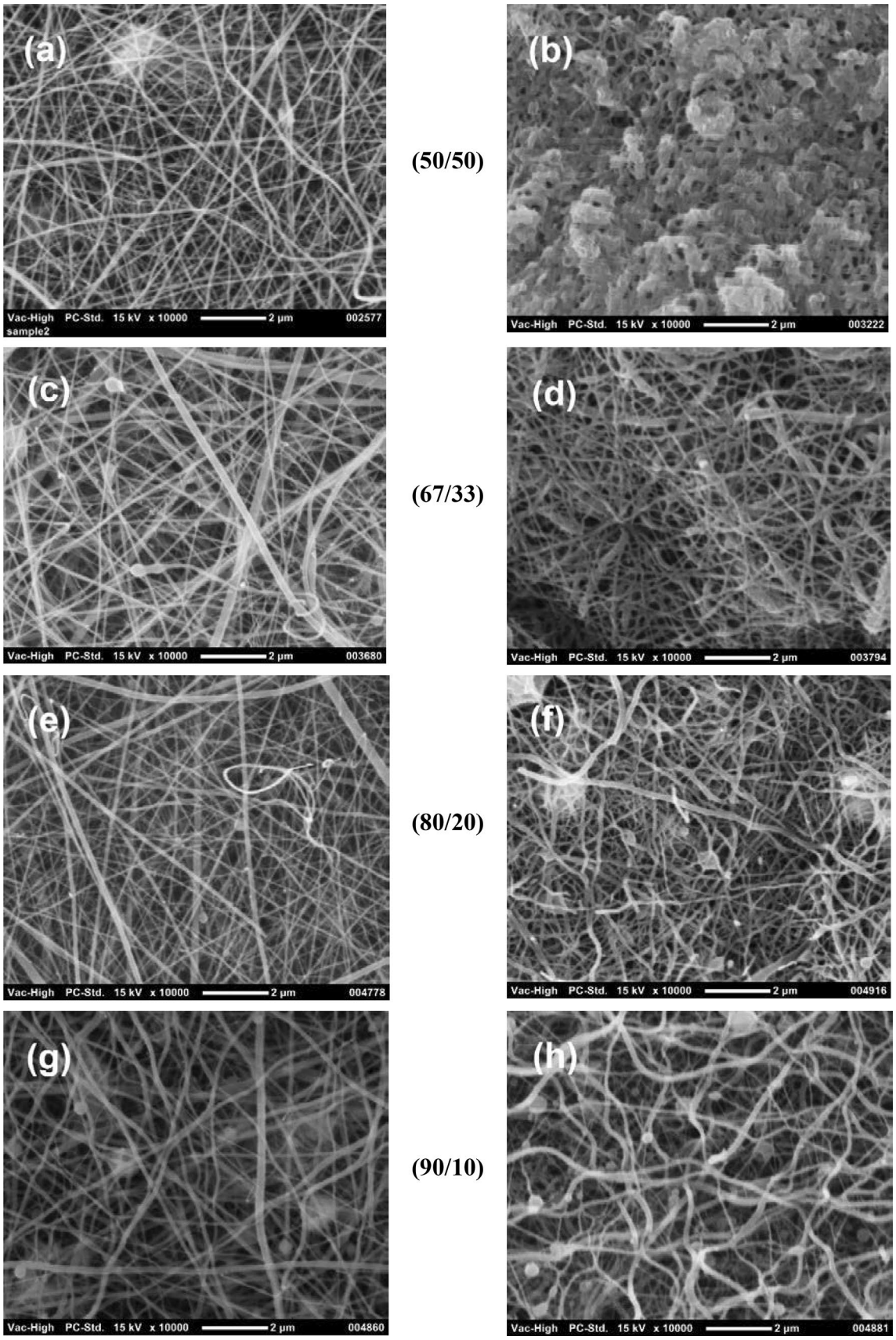
(a)
Vac-High PC-Std. 15 kV x 10000 2 µm 002577
sample2
(50/50)
(b)
Vac-High PC-Std. 15 kV x 10000 2 µm 003222
(c)
Vac-High PC-Std. 15 kV x 10000 2 µm 003680
(67/33)
(d)
Vac-High PC-Std. 15 kV x 10000 2 µm 003794
(e)
Vac-High PC-Std. 15 kV x 10000 2 µm 004778
(80/20)
(f)
Vac-High PC-Std. 15 kV x 10000 2 µm 004916
(g)
Vac-High PC-Std. 15 kV x 10000 2 µm 004860
(90/10)
(h)
Vac-High PC-Std. 15 kV x 10000 2 µm 004881

◂**Fig. 2** The morphology of the electrospun (left) and of the carbonized (right) electrospun nanofibers of minimum average diameter (< 100 nm). Scale bar in all SEM images is 2 μm

temperature range from 25 to 800 °C. Differential Scanning Calorimetry (DSC) tests were performed at inert atmosphere (N_2) with a heating rate of 7 °C/min, using a TA DSC25 instrument. The X-ray diffraction (XRD) patterns were recorded using a Philips X'Pert3 diffractometer with a Cu–Ka radiation source (1.54 Å).

Moreover, the textural properties (BET surface area and pore volume) of the activated carbon nanofibers were studied in connection to the lignin/r-PET mass ratio and to the average fiber diameter of the precursor electrospun nanofibers. For this purpose, the following electrospun samples were prepared; five samples consisting of 50/50 lignin/r-PET with D of 85 nm, of 230 nm, of 292 nm, of 395 nm and of 565 nm respectively; one sample consisting of 80/20 lignin/r-PET with D of 252 nm; finally, one sample consisting of 90/10 lignin/r-PET with D of 147 nm. Each of these samples was carbonized in the tubular furnace under inert atmosphere (N_2) at a heating rate of 5 °C/min until it reached 800 °C, where it was held for 1 h. Then the temperature was decreased to 600 °C, the gas was switched to CO_2, and the sample was activated for 1 h at this temperature. Finally, the gas was switched again to N_2 and left to cool down at room temperature. The textural characterization of the activated carbon nanofibers was studied through N_2 physisorption using a Micromeritics Tristar II Plus instrument. The surface area of each sample was calculated using the Brunauer–Emmet–Teller (BET) equation, the total pore volume was determined using the Gurvitch rule at $P/P_o = 0.95$ and the micropore volume was estimated using the t-plot approach. In addition, exactly the same procedure was followed for pristine lignin powder; it was carbonized at 800 °C with N_2, activated at 600 °C with CO_2 and its textural characteristics were measured for comparison, as well.

Results and discussion

The effect of the lignin/r-PET mass ratio

Whenever it is attempted to carbonize electrospun mats of submicron-sized and nano-sized fibers having different average diameters and prepared from varying lignin/r-PET mass ratios, we have repeatedly observed that at certain conditions the fibers melt to a smaller or larger extent, therefore, the filamentous structure collapses. When the degree of melting is extensive, then these electrospun samples yield a rigid, brittle chunk of char, which has lost its fibrous structure. In contrast, when there is only minor or negligible melting among the fibers, then these samples yield carbon nanofibrous mats which have some degree of flexibility and they retain their filamentous structure. Quantifying the degree of melting is not easy; thus, we decided to use a simple qualitative description by distinguishing three categories for the extent of melting; namely, "extensive", "moderate" and "minor". We term as "extensive" the degree of melting which results in the total collapse of the filamentous structure; in this case, most of the fibers have lost their shape and it is not possible to distinguish them. Typical examples of this behavior are presented in fig. S1 of the Supplementary Material. In "moderate" melting, there is an existing yet relatively limited extent of fusion, especially at the spots where many fibers form "knots". Here, there is a significant degree of interconnection among the fibers, but their shape is distinguishable. Typical examples of moderate melting are presented in fig. S2 of the Supplementary Material. Finally, when the degree of melting is very limited or hard to distinguish, we use the term "minor". There are signs of fusion at some spots where the fibers touch each other, but the degree of interconnection is very limited. Typical examples of minor melting are presented in fig. S3, and also in fig. S7 and S8 of the Supplementary Material. Although this is a subjective description and the limits between these categories are not well-defined, we believe that it offers a relatively precise overview of the behavior of the electrospun nanofibers upon heating, as it is apparent in the SEM images of Fig. 2.

Figure 2 presents the effect of the lignin/r-PET mass ratio in the carbonization of electrospun mats, in which the average fiber diameter is in the range of 80–100 nm, the lowest average fiber diameters produced successfully. The images on the left side correspond to the electrospun samples, while these on the right to the carbonized ones. Apparently, when the lignin/r-PET mass ratio is 50/50, which means that the percentage of r-PET in the fibers is relatively high, then there is an extensive degree of melting (Fig. 2a, b). The fibers have almost completely fused with each other, and the filamentous structure has collapsed. In contrast, at higher lignin/r-PET mass ratios, when the percentage of r-PET becomes progressively less, the degree of melting wanes. Thus, at 67/33 there is an extensive to moderate melting (Fig. 2c, d), at 80/20 a minor to moderate melting (Fig. 2e, f) and at 90/10 only a minor degree (Fig. 2g, h).

This behavior is justified by the differences in the macromolecular structure and in the thermal properties between these two polymers as PET is a linear, semicrystalline polymer with a melting point of around 250 °C, while the lignin used here is highly branched, amorphous and infusible when heated (Svinterikos et al. 2019). Therefore, it is expected that samples which contain a larger amount of r-PET will exhibit more extensive melting. In the samples of minor melting, the

resulting carbon nanofibers have average diameters similar to the precursor ones.

The synergy between the mass ratio and the average fiber diameter

The behavior described in the previous section is not uniform for the whole range of average fiber diameters at the sub-micron scale. As the average fiber diameter of the electrospun sample becomes larger, then the degree of melting becomes much less pronounced, even for samples that contain a large proportion of r-PET. In a recent article, we have shown that the average fiber diameter determines the carbonization outcome of fibers prepared from a 50/50 lignin/r-PET mass ratio (Svinterikos et al. 2019). In this case, electrospun samples of minimum average fiber diameter (~ 100 nm) melt extensively (as shown in Fig. 2b), while for electrospun samples with average diameter in the range of 200–300 nm the melting becomes moderate, and for samples whose average diameter is larger than 350–400 nm there is only a minor degree of fusion. Here, we extend this discussion for fibers prepared from a higher lignin/r-PET mass ratio, where the fiber diameter still plays a role, but of less significance as the mass ratio increases.

Figure 3 shows the carbonization results for the four mass ratios examined here, but for relatively thicker fibers. In Fig. 3a, b, it is apparent that the electrospun sample consisting of 50/50 lignin/r-PET with average fiber diameter of 387 nm exhibits a minor degree of fusion. So, the fibrous structure is retained and carbon submicron fibers are produced successfully. For electrospun samples consisting of 67/33 lignin/r-PET with an average diameter of 320 nm (Fig. 3c, d), it is obvious that there is only a moderate to minor melting, and definitely to a less extent compared to the thinner nanofibers shown in Fig. 2d. Similarly, fibers consisting of 80/20 lignin/r-PET with average diameter of 168 nm exhibit a rather minor degree of melting (Fig. 3e, f), while for fibers of 90/10 mass ratio the extent of melting is minor even for the thinnest fibers as shown in Fig. 2h and obviously, the same occurs for thicker fibers.

As the SEM images in Figs. 2 and 3 indicate and as we repeatedly observed when we carbonized samples of varying average fiber diameters and mass ratios, the samples consisting of the thinnest fibers tend to melt more extensively, and this degree of melting wanes as the average fiber diameter is increased and as the lignin/r-PET mass ratio is higher. Concisely, these observations are visualized in Fig. 4. Here, the darkest regions correspond to a higher degree of melting, while the lighter ones to a lower degree. The purpose of this figure is to provide a rough estimation and a better understanding, but not to set distinct and rigor limits between the regions. Here it must be mentioned, that we have repeatedly noticed that the melting in each sample is manifested even when it is heated under N_2 up to just 250–300 °C. Further heating to higher temperatures does not contribute to the extent of melting, but rather it only serves as the route to transform the samples into carbon fibers. In other studies where carbon fibers are produced from the carbonization of lignin, it is commonly suggested that including a stabilization step of heating in air at around 250 °C can help in preserving the filamentous structure (Ruiz-Rosas et al. 2010). However, adding a stabilization step here did not make any difference in the degree of fusion between the fibers, probably because this is caused by the presence of r-PET.

Moreover, it is necessary to mention that examining in detail what happens when the lignin/r-PET mass ratio is less than 50/50 is not of interest for our research. The reason is that we intend to prepare activated CNFs from lignin/r-PET and to use them for adsorption applications, therefore, it is preferable to have a high proportion of lignin in order to have a higher carbon yield and a well-formed filamentous structure. When we prepared electrospun submicron fibers of around 400 nm average diameter, consisting of a 40/60 lignin/r-PET ratio, we observed that during carbonization there was a moderate to extensive melting (fig. S4 in the Supplementary Material). We attribute this to the high content of r-PET. For the 40/60 mass ratio, we didn't prepare samples of different average fiber diameter to study their behavior. Instead, we chose to focus on samples containing less r-PET, for which we saw that we can produce thinner carbon nanofibers. Thus, we decided to focus on lignin/r-PET ratios between 50/50–90/10.

During carbonization, the decomposition of the lignin macromolecules proceeds in a multi-stage process, the first stage of which occurs in the region of 180–260 °C (Rodríguez Correa et al. 2017; Svinterikos et al. 2019). After the cleavage of the weaker bonds, the decomposition continues at higher temperatures, with the final stage occurring above 600 °C (Rodríguez Correa et al. 2017; Svinterikos et al. 2019). This multi-stage process is justified by the irregular structure of the lignin macromolecules. In contrast, the decomposition of r-PET occurs in a single stage close to 400 °C (Ko et al. 2014; Svinterikos et al. 2019). The decomposition profiles of the lignin/r-PET fibers include all these stages and they are presented in Fig. 5. In this figure, the weight loss and the decomposition rates of lignin/r-PET electrospun samples prepared from different mass ratios (50/50–90/10) can be seen, as they were monitored through thermogravimetry in the region between 50 and 800 °C. All of the samples presented here consist of nanofibers with similar average diameters (80–100 nm), the minimum range of average diameters produced successfully.

The results indicate that in the region between 180 and 260 °C (the first decomposition regime of lignin), the samples which contain a larger amount of lignin exhibit a higher weight loss and a slightly higher decomposition rate (see

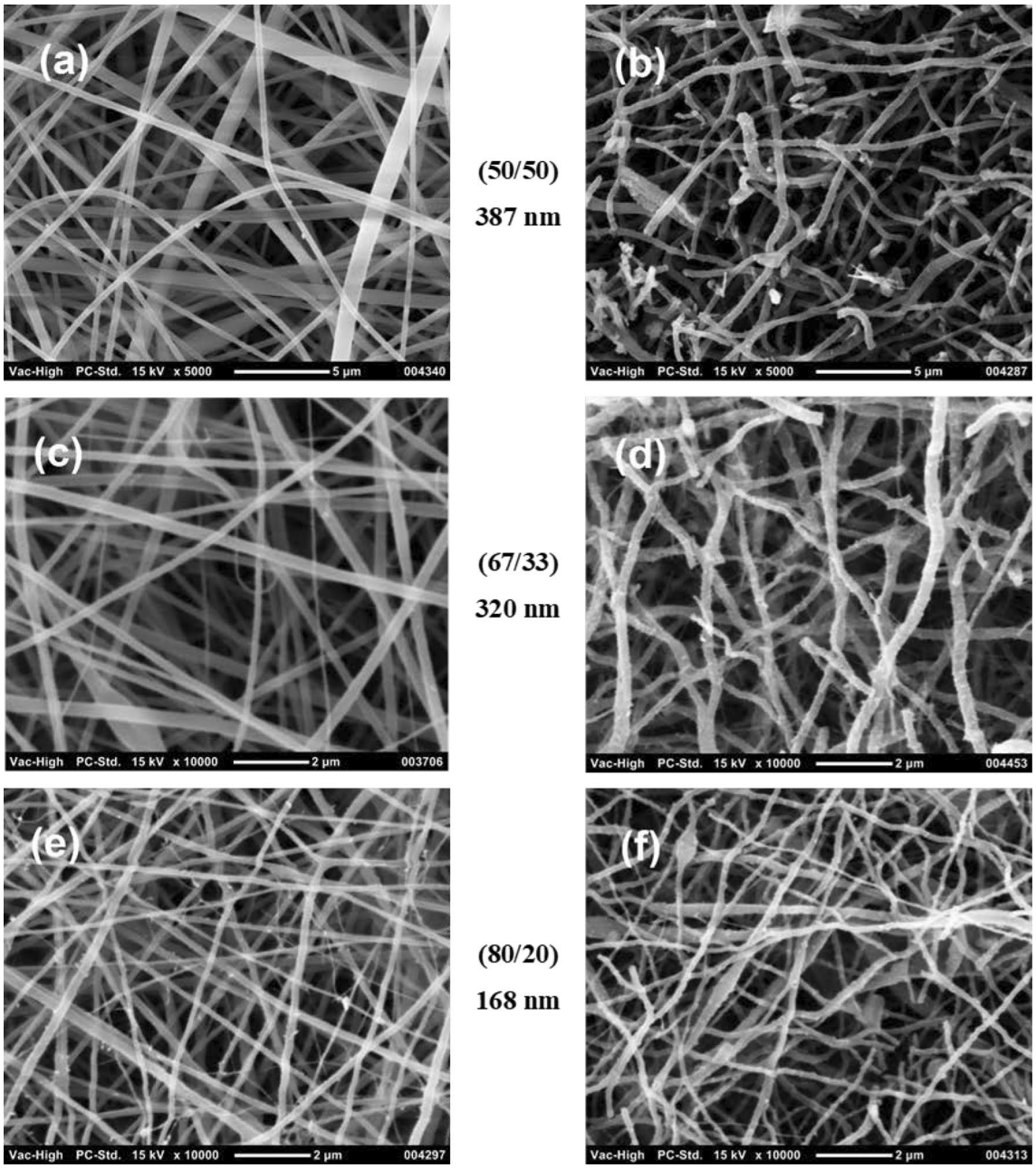

Fig. 3 SEM images showing the morphology of the electrospun (left) and of the carbonized (right) samples consisting of relatively thicker fibers. Scale bar in **a** and **b** is 5 µm; scale bar in the **c**–**f** is 2 µm

Table 1). In this region, the percent of weight loss for the sample of 50/50 is measured 14.5%, for the sample of 67/33 it is 17.2%, for the one of 80/20 it is 17.4% and for that of 90/10 it reaches the value of 19.2%. Similarly, the maximum decomposition rate (peak) in this region appears in the sample which contains the highest amount of lignin (90/10), and it is measured to be 0.45%/°C. The sample of 50/50 reaches a maximum rate of 0.40%/°C. Furthermore, in the region where the r-PET decomposes (330–470 °C), the sample containing the highest amount of r-PET shows the highest peak of decomposition (0.36%/°C) and the highest weight loss, while the other samples decompose at a significantly lower rate here.

Focusing on the samples with mass ratios 50/50 and 67/33, which melt to a larger extent when their average fiber diameter is minimum, a comparison of the thermogravimetric curves between samples of different average diameters illuminates the cause of this phenomenon. Figure 6 presents a comparison of the decomposition rates between samples of the minimum average fiber diameter (which melt to a

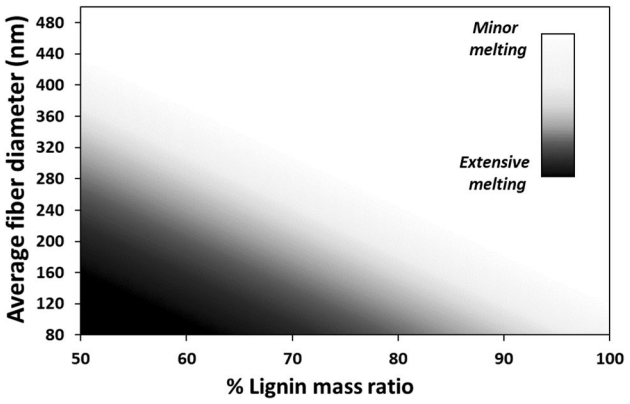

Fig. 4 The approximate degree of melting with regards to the lignin/r-PET mass ratio and to the average fiber diameter of the electrospun samples

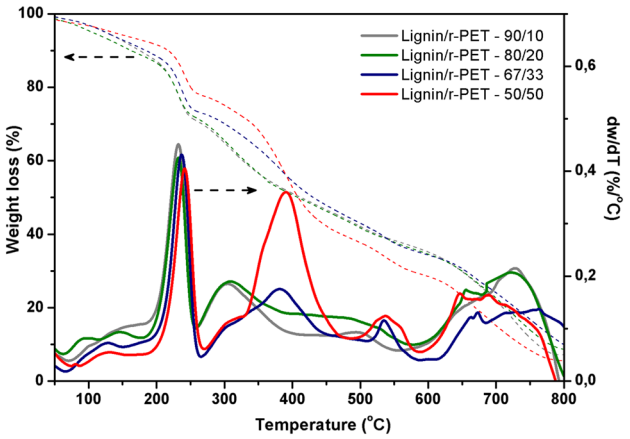

Fig. 5 The decomposition profiles of the lignin/r-PET electrospun nanofibers of minimum average diameter

Table 1 Thermogravimetric features in the region 180–260 °C (Fig. 5)

	Lignin/r-PET mass ratio			
	50/50	67/33	80/20	90/10
Weight loss (%)	14.5	17.2	17.4	19.2
Peak decomposition rate (%/°C)	0.40	0.43	0.43	0.45

larger extent) and samples of relatively larger average fiber diameter (which show a minor degree of melting) for these two mass ratios. This figure reveals that the samples of minimum average fiber diameter decompose at a significantly higher rate compared to those consisting of a larger average fiber diameter in the first region of lignin decomposition, i.e. between 180 and 260 °C. The features measured for these 4 samples are concisely presented in Table 2.

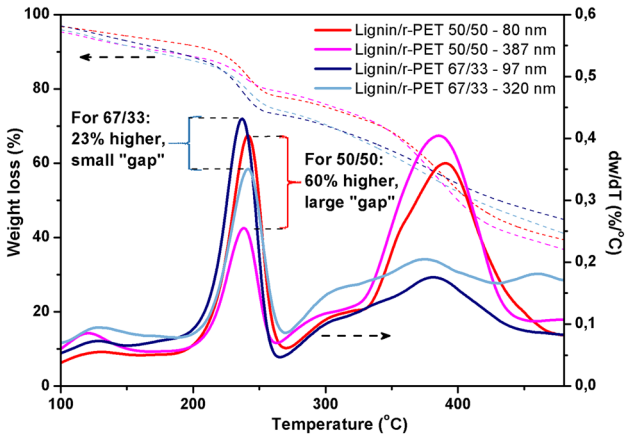

Fig. 6 The combined effect between the mass ratio and the average fiber diameter in the decomposition of lignin/r-PET electrospun nanofibers

Table 2 Thermogravimetric features in the region 180–260 °C: the synergy between mass ratio and average fiber diameter (Fig. 6)

	Mass ratio 50/50		Mass ratio 67/33	
	387 nm	80 nm	320 nm	97 nm
Max. decomposition rate (peak) (%/°C)	0.25	0.40	0.35	0.43

For the samples consisting of 50/50 lignin/r-PET, the nanofibers of 80 nm reach a maximum decomposition rate (peak) of 0.40%/°C, while those of 387 nm reach a peak of only 0.25%/°C. Similarly, for 67/33 lignin/r-PET the nanofibers of 97 nm reach a maximum rate of 0.43%/°C, while those of 320 nm reach a maximum rate of just 0.35%/°C (Table 2). It seems that as the lignin/r-PET mass ratio increases, the "gap" in the decomposition rate between the thinnest and the thicker fibers closes. Thus, for 50/50 lignin/r-PET the maximum rate reached by the thinnest fibers is 60% higher than the peak of the larger fibers, while for 67/33 the peak of the thinnest fibers is just 23% higher of the thicker ones (as noted on Fig. 6). This means that as the lignin/r-PET ratio increases, the difference in the decomposition rates between fibers of different diameters decreases, and the effect of the diameter becomes less significant. This observation explains why at high lignin/r-PET ratios the degree of melting doesn't vary much among fibers of different diameters (Figs. 2, 3).

The carbonization process involves the transfer of heat from the surface towards the bulk of the fiber and also the transfer of mass (the volatile products) from the bulk of the fiber towards the surface and to the atmosphere. Therefore, it is a process controlled by heat and mass transfer restrictions. When the fiber diameter is minimized, then its specific

surface area is maximized (the external surface without taking into account any porosity, a valid assumption here as the electrospun fibers are not porous). In addition, when the fiber diameter is reduced, more molecules are located at or near the surface. So, it is expected that in the case of very thin fibers the heat and mass transfer limitations are less pronounced, and the overall rate of the process is mostly controlled by the decomposition reactions occurring on the surface and in the bulk of the fibers. In contrast, when the fibers are relatively thicker, the overall rate is limited by the heat and mass transfer rates. This assumption is confirmed by the thermogravimetric curves shown in Fig. 6, comparing the differences in the decomposition rates between thicker and thinner fibers.

At high lignin/r-PET mass ratios, there is a higher percentage of lignin macromolecules on the surface and inside the fibers. As the nanofibers are heated, they reach the region of 180–260 °C, and lignin starts to decompose. When the fibers contain a higher percentage of lignin, it seems that the lignin decomposition reactions themselves are more significant than the heat and mass transfer for the overall rate of the process, because less r-PET macromolecules are present and, so, they hinder to a lesser extent the decomposition of lignin. The hindering effect of the r-PET is based on the fact that they occupy parts of the fiber surface, and also by the fact that they absorb energy in this region (180–260 °C) without decomposing. Therefore, at higher lignin/r-PET mass ratios, the mass ratio itself becomes more important than the fiber diameter, as it is shown in the thermogravimetric results of Fig. 6 and also in the morphologies of Figs. 2 and 3. To the best of our knowledge, this is the first time that the combining effect between the mass ratio and the average fiber diameter has been reported to determine the morphology of the carbonized fibers, when a blend of polymers is used as feedstock.

The differences in the decomposition of lignin between 180 and 260 °C are crucial for understanding the distinct melting behavior of each sample, as it will be shown in the following results from XRD and DSC. As r-PET consists of linear macromolecular chains, when lignin and r-PET are mixed then the branched macromolecules of lignin restrict the movement of r-PET chains and they hinder its crystallization (Svinterikos and Zuburtikudis 2016). The extent of this hindrance depends on the mass ratio of lignin.

When pure r-PET is used, the r-PET nanofibers prepared from the electrospinning process are amorphous, as it is revealed when they are examined with XRD (Fig. 7). This is not unexpected; instead, this has been reported in the literature in several occasions (Mazinani et al. 2010; Thomas et al. 2018) not only for PET but for other polymers as well (Ko and Wan 2014b). This absence of crystallinity in the as-prepared r-PET nanofibers can be explained by the rapid solidification process during electrospinning (Ko and Wan

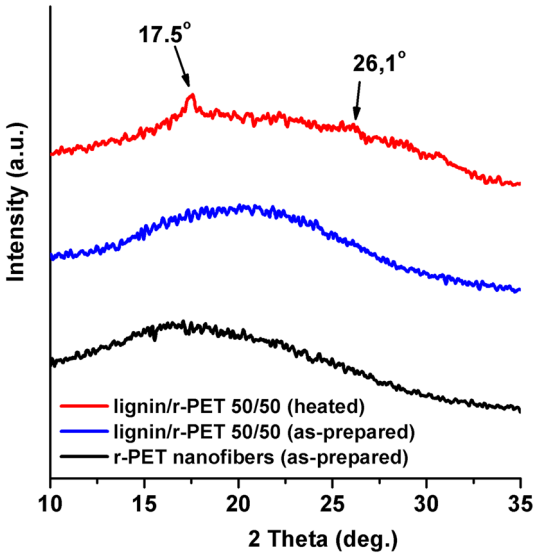

Fig. 7 X-ray diffraction patterns of electrospun nanofibers prepared from pure r-PET, from 50/50 lignin/r-PET (as-prepared) and from 50/50 lignin/r-PET after heating them at 300 °C (the curves have been displaced on the *y*-axis)

2014b). However, when these r-PET nanofibers are heated, they totally melt at around 250 °C, because they pass through a crystallization phase at around 150–190 °C (Svinterikos and Zuburtikudis 2016; Thomas et al. 2018). As a certain amount of lignin is mixed with r-PET (e.g. 30–40%), the crystallinity being developed in this region is compromised. When the percentage of lignin is increased, then the crystallization shifts towards higher temperatures and it becomes less apparent in the DSC thermograms until it is practically undetected when the lignin/r-PET mass ratio is higher than 67/33 (Svinterikos and Zuburtikudis 2016). However, the fact that lignin starts to decompose above 180 °C probably gives the chance to r-PET chains to gain some mobility and to re-organize to a small extent at some regions (Svinterikos et al. 2019), especially when the fiber diameter is minimum and the lignin decomposition rate becomes maximum. Therefore, when the electrospun samples reach temperatures between 220 and 250 °C, there is some extent of melting. The fact that more lignin decomposes when the sample consists of thin nanofibers (~ 80–100 nm) compared to samples consisting of thicker fibers (Fig. 6), probably means that the r-PET chains gain more space to re-organize, therefore, these samples exhibit a higher degree of melting compared to the samples which contain thicker submicron fibers. This behavior is more pronounced for samples consisting of lignin/r-PET mass ratio of 50/50, but it also occurs for samples of 67/33 even to a smaller extent.

This phenomenon can be better understood when an electrospun sample is heated to 300 °C under N_2 and then left to cool down at room temperature. In this case, a portion

of lignin has decomposed, while the r-PET chains have not. Therefore, there can be a detectable difference in the crystallinity between the as-prepared electrospun sample and the sample heated at 300 °C. This difference can be seen in Fig. 7 for a sample consisting of 50/50 lignin/r-PET, with average fiber diameter of 80 nm. The as-prepared sample doesn't contain any peaks. However, when it is heated at 300 °C and then left to cool down, two peaks emerge; a larger one at $2\theta = 17.5°$ and a broad smaller one at $2\theta = 26.1°$. These peaks correspond to characteristic patterns of the crystal planes of PET [the first peak to (010) and the second one to (100), respectively] (Sun et al. 2018; Dong et al. 2019). This implies that the sample undergoes some small extent of crystallization as it is heated, which is obviously enhanced by the decomposition of lignin above 180 °C.

Investigation with DSC can contribute to a further understanding of these phenomena. Again, these measurements were conducted for the electrospun samples which were heated at 300 °C under N_2, then left to cool down and afterwards they were examined with DSC. In Fig. 8, the DSC thermograms are presented for four samples in the region of 170–270 °C, the region where the melting peak is expected to appear. The samples shown here are two samples of lignin/r-PET with mass ratio 50/50 and average fiber diameter of 80 nm and of 387 nm, one sample of 67/33 lignin/r-PET with average fiber diameter of 97 nm and one sample consisting of 80/20 lignin/r-PET with average fiber diameter of 95 nm. The curves corresponding to the two 50/50 lignin/r-PET samples were presented in a previous article of our team (Svinterikos et al. 2019) and are shown here again for comparison purposes. These DSC curves illuminate the differences in the melting of the samples based on their average diameter and on their mass ratio. The curves of the samples consisting of 50/50 lignin/r-PET exhibit broad melting peaks in the region of 220–250 °C. Between these two, the sample of minimum diameter exhibits a larger melting peak, and the enthalpy of melting is measured to be around 1.2 J/g (Svinterikos et al. 2019). The other sample, which consists of thicker fibers has a smaller melting peak and an enthalpy of melting of 0.4 J/g (Svinterikos et al. 2019). The differences between these two peaks are illuminating the effect of the nano-diameter in the extent of melting. The sample of 67/33, which consists of thin nanofibers, shows a very broad and small melting peak between 210 and 240 °C. This indicates that even when the amount of lignin is twice as large as the amount of r-PET in the sample, there is some minor rearrangement of some parts of the r-PET chains and some degree of melting as it is shown in Fig. 2, due to the higher decomposition rate of lignin appearing when the sample consists of thin nanofibers. The enthalpy of melting here was measured to be around 0.1 J/g. In contrast, when the percentage of lignin is even higher (80%) which means that the sample contains four times more lignin than PET, there is no detectable melting peak.

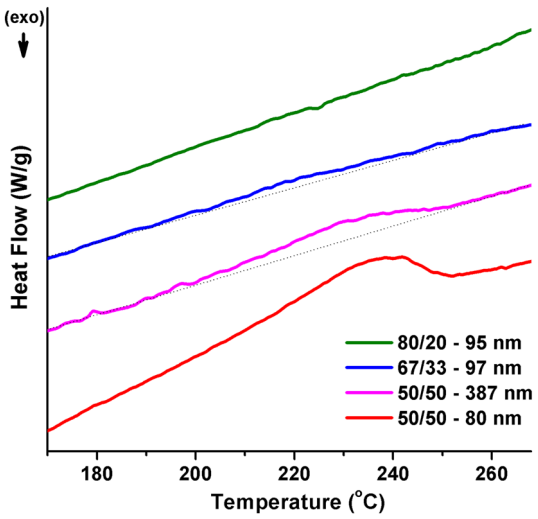

Fig. 8 DSC curves of electrospun samples after they were heated up to 300 °C under N_2. The dotted straight lines were added for the ease of comparison. (The curves have been displaced on the *y*-axis)

Here, we should underline that the emergence of some degree of melting is not necessarily a drawback. Dallmeyer et al. prepared carbon nanofibers derived from lignin-based electrospun nanofibers (Dallmeyer et al. 2014). Using different types of lignin, he prepared carbon nanofibers with some degree of inter-connection due to fusion. The fusion was the result of the structural differences among the different types of lignin used. It was shown that the inter-fiber bonding improved the tensile strength and the electrical conductivity of the carbon fibrous samples. However, in our study we use a single type of lignin (infusible when heated) and we have shown that the fusion comes from the presence of r-PET.

Textural characterization of the activated CNFs

After mapping the conditions that are necessary for the avoidance of melting, it was necessary to investigate if the melting influences the porosity of the carbon nanofibrous mats. For this purpose, seven samples were prepared, carbonized and activated as described in Sect. 2 (experimental part) and their porosity and BET surface area were measured. For comparison, the same procedure was followed for pristine lignin powder, as well. The results are displayed in Table 3. The two samples consisting of 80/20 and of 90/10 lignin/r-PET were fabricated with such average fiber diameters, to avoid melting and to assess how the lignin/r-PET mass ratio affects the porosity. The N_2 physisorption isotherms as well as representative SEM images of these samples are shown in the Supplementary Material (fig. S5–S8).

Table 3 Textural characterization of the activated carbon nanofibers

Sample ID		Results		
Lignin/r-PET mass ratio	Average fiber diameter (nm)	BET surface area (m^2/g)	Total pore volume (cm^3/g)	Micropore volume (cm^3/g)
50/50	85	72	0.060	0.028
50/50	230	123	0.112	0.046
50/50	292	132	0.109	0.052
50/50	395	288	0.194	0.116
50/50	565	276	0.182	0.108
80/20	252	210	0.136	0.079
90/10	147	216	0.133	0.089
100/0 (pure lignin)	–	176	0.091	0.079

The results clearly indicate that in the samples consisting of 50/50 mass ratio the degree of melting influences the development of porosity. The highest values of BET surface area and of total pore volume appear for the samples that remain infusible (average fiber diameter > 395 nm). Moreover, it seems that increasing the average fiber diameter from 395 to 565 nm doesn't affect the porosity significantly, as the BET surface area ranges between 276 and 288 m^2/g and the total pore volume between 0.182 and 0.194 cm^3/g. In contrast, when the nanofibrous mats consist of thinner fibers that melt (< 292 nm) the BET surface area does not increase more than 132 m^2/g.

In addition, the lowest porosity and BET surface area appears for the sample that exhibits the most extensive melting. After such a sample is carbonized, it appears as a solid chunk of carbon; since the lignin and the r-PET decompose anyway during carbonization, obviously closed pores are created which are inaccessible to N_2. On the contrary, when the samples remain infusible the different nanofibrous horizontal layers can be separated by friction and they are more flexible. For the samples which remain infusible, the average fiber diameters of the CNFs remain at similar levels as the precursor electrospun nanofibers.

Furthermore, although the samples of higher lignin content (80/20 and 90/10) consist of almost infusible thin nanofibers, their porosity lies in the range between 0.133 and 0.136 cm^3/g which is much less compared to the infusible 50/50 samples. Based on these measurements, it seems that the r-PET functions as a sacrificial, porosity-generating template. The r-PET macromolecules decompose to a larger extent than lignin (Svinterikos et al. 2019). Measurements with thermogravimetric analysis have shown that the starting recycled PET leaves a residue of less than 10 wt% at 800 °C, while the residue of pristine lignin powder is close to 35 wt% (Svinterikos et al. 2019). In the case of lignin/r-PET nanofibers, the decomposition of the r-PET macromolecules leaves voids which translate into porosity, hence, when the r-PET content is larger the porosity is higher. This has also been reported for other lignin-based electrospun-derived carbon nanofibers, in which lignin was combined with poly(vinyl alcohol) (Ago et al. 2016; Beck et al. 2017) or polyvinylpyrrolidone (Ma et al. 2018). In these cases, the binder polymer acted sacrificially for porosity development, as well.

Compared to the carbonized and activated pristine lignin powder, the infusible carbon nanofibers contain higher porosity. Moreover, in contrast to pristine lignin powder which yields highly microporous granular activated carbon, the activated carbon nanofibers contain significant mesoporosity, as it is obvious by comparing the micropore volume to the total pore volume for each sample, and by inspection of their N_2 isotherms which are type IV with hysteresis loops (Supplementary Material, figs. S5 and S6). The granular activated carbon produced by lignin gives a type I isotherm, typical of a microporous material. The morphology of this granular activated carbon is shown in fig. S9 of the Supplementary Material.

Conclusions

The ability to produce carbon nanofibers with custom-made, on-demand morphologies can be a decisive factor for the applicability of this high-value engineering material. In this study, we have demonstrated that when carbon nanofibers from a blend of lignin with r-PET are produced, their fibrous morphology can be customized by properly adjusting the lignin/r-PET mass ratio and the average diameter of the precursor nanofibers. Very fine CNFs with average diameters close to 100 nm are among the lowest reported when lignin is used as precursor. To the best of our knowledge, this is also the first time that the synergy between the mass ratio and the average fiber diameter has been described as a crucial factor when carbon nanofibers are prepared from a blend of two polymers. When the mass ratio is roughly between 50/50 and 67/33, there is a considerable degree of melting during the carbonization of precursor nanofibrous mats with

low average diameters (lower than 200 nm). The reason is that the thinnest nanofibers decompose with a higher rate between 180 and 260 °C, the region of lignin decomposition, and consequently the mobility of the r-PET chains inside the fibers becomes less restricted. Thus, the r-PET chains can re-arrange to a larger extent and the nanofibers merge with each other when they reach the melting temperature region of r-PET (220–250 °C). For this range of mass ratios, the fusion of fibers is minimized when the average fiber diameter of the mats is increased above 300–400 nm. In contrast, when the lignin/mass ratio approaches the value of 90/10, then the precursor nanofibers tend to retain their filamentous morphology even when the average fiber diameter is low, therefore, it is feasible to produce lignin-based carbon nanofibrous mats with average diameter close to 100 nm. At such lignin/r-PET mass ratios, the amount of lignin is so high that it prevents the r-PET chains from crystallizing, and thus, the melting can be avoided. When the carbon nanofibers are designed for a specific application in which some degree of fusion is beneficial (e.g. for electrical applications, in which the electrical conductivity is important), then the fusion can be accordingly controlled to achieve the desired result. Furthermore, the porosity and the BET surface area of the carbon nanofibers are compromised when the precursor nanofibers melt during carbonization. In addition, the r-PET functions as a porosity-generating template, therefore, the highest BET surface area and porosity appear in carbon nanofibers derived from a 50/50 lignin/r-PET mass ratio with average fiber diameters in the infusible region (> 400 nm).

This study highlights the factors that should be taken into account when a desired carbon fibrous morphology is fabricated, and it illuminates their role. Moreover, these results provide a roadmap for the successful production of carbon nanofibers from inexpensive, renewable and waste resources. Therefore, this study can contribute to the development of more economically produced carbon nanofibers, and to the promotion of their wider use.

Acknowledgements The authors would like to acknowledge the financial support provided by the Emirates Center for Energy and Environment Research (Grant number 31R147).

Compliance with ethical standards

Conflict of interest On behalf of all authors, the corresponding author states that there is no conflict of interest.

References

Ago M, Borghei M, Haataja JS, Rojas OJ (2016) Mesoporous carbon soft-templated from lignin nanofiber networks: Microphase separation boosts supercapacitance in conductive electrodes. RSC Adv 6:85802–85810. https://doi.org/10.1039/c6ra17536h

Alekhina M, Erdmann J, Ebert A et al (2015) Physico-chemical properties of fractionated softwood kraft lignin and its potential use as a bio-based component in blends with polyethylene. J Mater Sci 50:6395–6406. https://doi.org/10.1007/s10853-015-9192-9

Baker DA, Rials TG (2013) Recent advances in low-cost carbon fiber manufacture from lignin. J Appl Polym Sci 130:713–728. https://doi.org/10.1002/app.39273

Beck RJ, Zhao Y, Fong H, Menkhaus TJ (2017) Electrospun lignin carbon nanofiber membranes with large pores for highly efficient adsorptive water treatment applications. J Water Process Eng 16:240–248. https://doi.org/10.1016/j.jwpe.2017.02.002

Choi DI, Lee J-N, Song J et al (2013) Fabrication of polyacrylonitrile/lignin-based carbon nanofibers for high-power lithium ion battery anodes. J Solid State Electrochem 17:2471–2475. https://doi.org/10.1007/s10008-013-2112-5

Dallmeyer I, Lin LT, Li Y et al (2014) Preparation and characterization of interconnected, kraft lignin-based carbon fibrous materials by electrospinning. Macromol Mater Eng 299:540–551. https://doi.org/10.1002/mame.201300148

Dong S, Jia Y, Xu X et al (2019) Crystallization and properties of poly(ethylene terephthalate)/layered double hydroxide nanocomposites. J Colloid Interface Sci 539:54–64

Duval A, Lawoko M (2014) A review on lignin-based polymeric, micro- and nano-structured materials. React Funct Polym 85:78–96. https://doi.org/10.1016/j.reactfunctpolym.2014.09.017

Frank E, Steudle LM, Ingildeev D et al (2014) Carbon fibers: precursor systems, processing, structure, and properties. Angew Chemie Int Ed 53:5262–5298. https://doi.org/10.1002/anie.201306129

García-Mateos FJ, Cordero-Lanzac T, Berenguer R et al (2017) Lignin-derived Pt supported carbon (submicron) fiber electrocatalysts for alcohol electro-oxidation. Appl Catal B Environ 211:18–30. https://doi.org/10.1016/j.apcatb.2017.04.008

Inagaki M, Yang Y, Kang F (2012) Carbon nanofibers prepared via electrospinning. Adv Mater 24:2547–2566. https://doi.org/10.1002/adma.201104940

Jin J, Yu BJ, Shi ZQ et al (2014) Lignin-based electrospun carbon nanofibrous webs as free-standing and binder-free electrodes for sodium ion batteries. J Power Sour 272:800–807. https://doi.org/10.1016/j.jpowsour.2014.08.119

Jönsson P, Evangelopoulos P, Persson H, Han T, Sophonrat N, Yang W (2018) Evolution of sulfur during fast pyrolysis of sulfonated Kraft lignin. J Anal Appl Pyrolysis 133:162–168. https://doi.org/10.1016/j.jaap.2018.04.006

Kadla JF, Kubo S (2004) Lignin-based polymer blends: analysis of intermolecular interactions in lignin–synthetic polymer blends. Compos Part A Appl Sci Manuf 35:395–400. https://doi.org/10.1016/j.compositesa.2003.09.019

Ko F, Wan Y (2014a) Introduction to nanofiber materials, Chapter 3. Cambridge University Press, Cambridge

Ko F, Wan Y (2014b) Introduction to nanofiber materials, Chapter 6. Cambridge University Press, Cambridge

Ko K, Rawal A, Sahajwalla V (2014) Analysis of thermal degradation kinetics and carbon structure changes of co-pyrolysis between macadamia nut shell and PET using thermogravimetric analysis and 13 C solid state nuclear magnetic resonance. Energy Convers Manag 86:154–164. https://doi.org/10.1016/j.enconman.2014.04.060

Lallave M, Bedia J, Ruiz-Rosas R et al (2007) Filled and hollow carbon nanofibers by coaxial electrospinning of Alcell lignin without binder polymers. Adv Mater 19:4292–4296. https://doi.org/10.1002/adma.200700963

Ma C, Li Z, Li J et al (2018) Lignin-based hierarchical porous carbon nanofiber films with superior performance in supercapacitors.

Appl Surf Sci 456:568–576. https://doi.org/10.1016/j.apsusc.2018.06.189

Mazinani S, Ajji A, Dubois C (2010) Fundamental study of crystallization, orientation, and electrical conductivity of electrospun PET/carbon nanotube nanofibers. J Polym Sci Part B Polym Phys 48:2052–2064. https://doi.org/10.1002/polb.22085

Mohabeer C, Reyes L, Abdelouahed L, Marcotte S, Taouk B (2019) Investigating catalytic de-oxygenation of cellulose, xylan and lignin bio-oils using HZSM-5 and Fe-HZSM-5. J Anal Appl Pyrolysis 137:118–127. https://doi.org/10.1016/j.jaap.2018.11.016

NAPCOR (2018) National association for PET container resources of USA. https://www.napcor.com/PET/landing_petrecycling.html. Accessed 20 Mar 2018

Peng S, Li L, Kong J et al (2016) Electrospun carbon nanofibers and their hybrid composites as advanced materials for energy conversion and storage. Nano Energy 22:361–395. https://doi.org/10.1016/j.nanoen.2016.02.001

Rodríguez Correa C, Stollovsky M, Hehr T et al (2017) Influence of the carbonization process on activated carbon properties from lignin and lignin-rich biomasses. ACS Sustain Chem Eng 5:8222–8233. https://doi.org/10.1021/acssuschemeng.7b01895

Ruiz-Rosas R, Bedia J, Lallave M et al (2010) The production of submicron diameter carbon fibers by the electrospinning of lignin. Carbon 48:696–705. https://doi.org/10.1016/j.carbon.2009.10.014

Sun P, Lu H, Zhang W et al (2018) Poly(ethylene terephthalate): rubbish could be low cost anode material of lithium ion battery. Solid State Ionics 317:164–169. https://doi.org/10.1016/j.ssi.2018.01.024

Svinterikos E, Zuburtikudis I (2016) Carbon nanofibers from renewable bioresources (lignin) and a recycled commodity polymer [poly(ethylene terephthalate)]. J Appl Polym Sci 133:43936. https://doi.org/10.1002/app.43936

Svinterikos E, Zuburtikudis I (2017) Tailor-made electrospun nanofibers of biowaste lignin/recycled poly(ethylene terephthalate). J Polym Environ 25:465–478. https://doi.org/10.1007/s10924-016-0806-3

Svinterikos E, Zuburtikudis I, Al-Marzouqi M (2019) The nanoscale dimension determines the carbonization outcome of electrospun lignin/recycled-PET fibers. Chem Eng Sci 202:26–35. https://doi.org/10.1016/j.ces.2019.03.013

Thakur VK, Thakur MK, Raghavan P, Kessler MR (2014) Progress in green polymer composites from lignin for multifunctional applications: a review. ACS Sustain Chem Eng 2:1072–1092. https://doi.org/10.1021/sc500087z

Thomas D, Schick C, Cebe P (2018) Novel method for fast scanning calorimetry of electrospun fibers. Thermochim Acta 667:65–72. https://doi.org/10.1016/j.tca.2018.07.001

Wang C-Q, Wang H, Liu Y-N (2015) Separation of polyethylene terephthalate from municipal waste plastics by froth flotation for recycling industry. Waste Manag 35:42–47. https://doi.org/10.1016/j.wasman.2014.09.025

Wool RP, Sun XS (2005) Bio-based polymers and composites. Bio-Based Polym Compos. https://doi.org/10.1016/B978-012763952-9/50017-4

Zhang M, Resende FLP, Moutsoglou A, Raynie DE (2012) Pyrolysis of lignin extracted from prairie cordgrass, aspen, and Kraft lignin by Py-GC/MS and TGA/FTIR. J Anal Appl Pyrolysis 98:65–71. https://doi.org/10.1016/j.jaap.2012.05.009

Zhang B, Kang F, Tarascon J, Kim J (2016) Recent advances in electrospun carbon nanofibers and their application in electrochemical energy storage. Prog Mater Sci 76:319–380. https://doi.org/10.1016/j.pmatsci.2015.08.002